Chapter 8: Interaction of Molecular Nanoparticles and CdS nanoparticles

Fluorescence quenching of nanoparticles of porphyrins [T(*p*-Cl)PP] and nanoparticles of metal-porphyrins [Zn-T(*p*-Cl)PP] in colloidal CdS

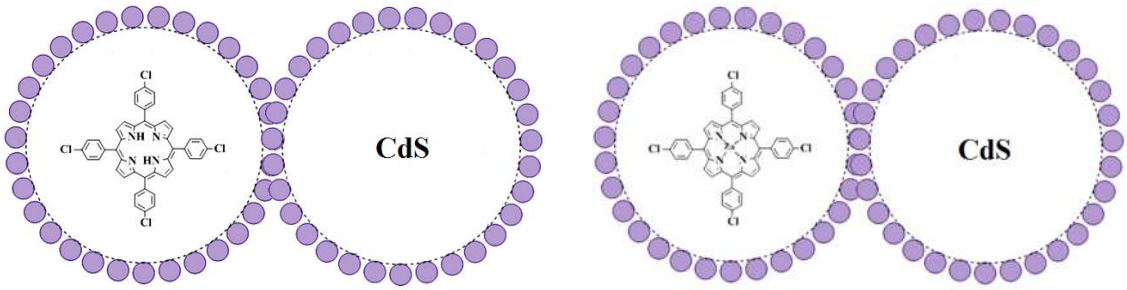

Photosensitization of stable, large band-gap semiconductors using dyes in the visible light has been subject of an active investigation [1]. Photosensitization can be achieved by adsorption of dye (sensitizer) molecules on the semiconductor surface by electrostatic, hydrophobic, or chemical interactions that, upon excitation, inject an electron into its conduction band [2]. The opto-electronic performance can be further improved by finely controlling the size and shape of organic nanostructures [3].

Formation of nanostructures from semiconductors and organic dye molecules results in a class of new materials which will be important for photovoltaic [4] and fluorescence markers in biological or medical applications [5].

Porphyrin/ metalloporphyrins having high extinction coefficients in the visible region finds increasing importance in catalysis, biochemistry, and photochemistry and it stand unique among these dyes. Several groups have studied physical and chemical processes of porphyrins on the different colloid surface [6].The spectrophotometric characteristics of the porphyrin are dictated by its binding or interaction with neighboring particle [7]. This leads to change in energy of the ground and excited states for electron or change transfer process. Due to very strong absorption in 400 –450 nm region (Soret band) and in the 500 –700 nm region (Q band), porphyrin/ metalloporphyrins attracted attention as a efficient photo sensitizer. They contain delocalized π-electrons, a necessary condition for easy electron transfer during the photo-interaction. Chemical reactivity between a porphyrin and other molecule involves either direct docking/binding of the two compounds or the formation of a reactive intermediate (e.g., proton, activated oxygen, etc.) that moves between the two non-complexes molecules [8].

.

Motivation: Interaction of inorganic nanoparticles with organic molecules is studied well in literature [9]. But what will happen if inorganic nanoparticles cross line with organic nanoparticles?

Studies on Tetraphenyl Porphyrin (TPP) and Metallo Tetraphenyl Porphyrin (TPP)

Abstract:

In part-I of this chapter, we have prepared *5,10,15,20*-tetra (4-chlorophenyl*)*porphyrin (**1**) and Zinc (II)-*5,10,15,20*-tetra(4-chlorophenyl*)*porphyrin (**Zn-1**). Synthesized compounds were characterized using elemental analyses, FT-IR, ^{1}H NMR, UV-Visible spectroscopy and fluorescence spectroscopy.

In part II, we have synthesized nanoparticles **1NP, Zn-1NP** from compounds **1** and **Zn-1**, respectively. We also synthesized nanoparticles of CdS (**3**). We found Polyacrylamide acts as a better stabilizer in comparison to various other stabilizers. All the synthesized **1NP, Zn-1NP** and **3** were characterized using DLS for their particle size in solution.

We report here interaction of **1NP/Zn-1NP**, as photosensitizers, with nanoparticles of CdS (**3**) by employing absorption and fluorescence techniques. *ex-situ* mixing of these solutions resulted in the large particle size (> 100nm) of resulting nanocomposite. Hence, *in-situ* syntheses of nanocomposite of **1NC**/**Zn-1NC** with CdS nanoparticles (**3**) were employed. Absorption spectra displayed formation of nanocomposite. We observed addition of CdS particles (**3**) results into total quenching of fluorescence emission of **1**/**1NP** and **Zn-1**/**Zn-1NP**. The fluorescence quenching is attributable mainly to excited state complex formation.

8.1 Introduction:

Porphyrins are cyclic tetrapyrrole derivatives in which four pyrrole or substituted pyrrole rings joined by sp^2 hybridized carbon atoms [10]. They are derived from parent compound porphine, by substitution of pyrrole exohydrogens 1,2,3,4,5,6,7 and 8 and the methine hydrogen's ***α, β, γ*** and ***δ***. Thus they can exist in varied forms by having different peripheral substituent's, eight pyrrole β -carbon atoms and the four meso-carbon centers. The skeleton structure of a porphine is represented in scheme 8.1.

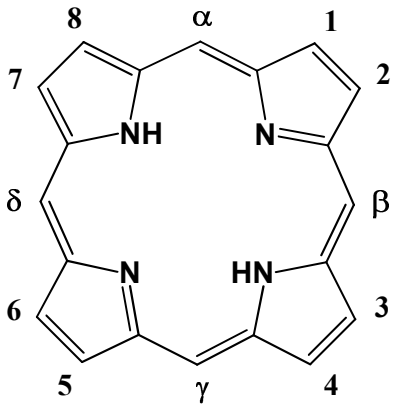

Scheme 8.1: Structure of porphine

The electronic heart of a free base porphyrin is the highly conjugated planar π-framework. There are 18 π-electrons in the cycle and hence the free-base porphyrin can be considered as 18-centre 18-electron cyclic polyene system. The inner 16 membered ring is structured with a basic 4-fold symmetry including 4-nitrogen atoms directed towards the centre.

Porphyrins are ubiquitous in natural systems and have potential applications in catalytic reactions, enzymes mimicking, molecular electronic devices and conversion of solar energy (photochemistry). Porphyrins exhibit key roles in nature. Reason behind this is their absorption, emission, charge transfer and complexing properties with various metals and compounds.

Electronic absorption spectra of porphyrins showed two types of intense bands, one in the 370–500 nm range, called Soret or B-band (molar extinction coefficients- 10^5 $M^{-1}cm^{-1}$) and other at longer wavelength, in the range-500–750-nm, called Q band (molar extinction coefficients of 10^4 $M^{-1}cm^{-1}$). Since, absorption bands are extensively overlapped with solar radiation, results into efficient conversion of radiation energy into

chemical energy.

Metalloporphyrin (scheme 8.2) complexes also play significant role in many biological and catalytic systems. Variety of metals can bind or fit into the "pocket" of the porphyrin ring system allowing functional diversity in metalloporphyrins.

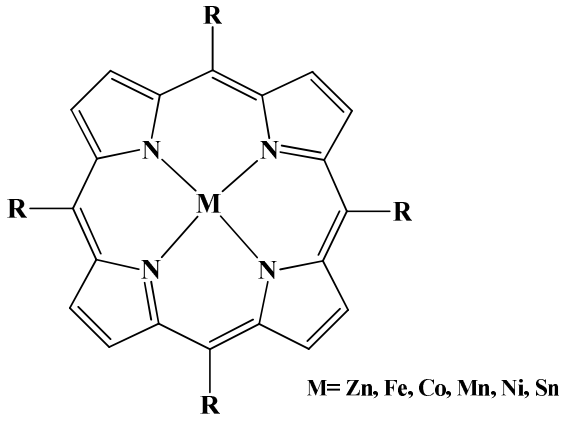

Scheme 8.2: Structure of Metalloporphyrin

Basically mettalloporphyrins are divided into two groups based on their UV-vis and fluorescence properties [11].

1. ***Regular* mettalloporphyrins:** It contains closed-shell metal ions (d^0 or d^{10}) such as Zn^{II}, in which the d_π (*dxz*, *dyz*) metal-based orbital's are relatively low in energy. It showed modest effect on the porphyrin energy gap (π to π^*) in porphyrin electronic spectra.
2. ***Hypsoporphyrins***: These are mettalloporphyrins in which the metals are of d^m (m = 6–9) having filled d_π orbital. In hypsoporphyrins there is significant metal d_π to porphyrin π^* orbital interaction (metal to ligand π-back bonding). Hence increase in π to π^* energy separation in porphyrin normally results in hypsochromic (blue) shifts in electronic absorptions.

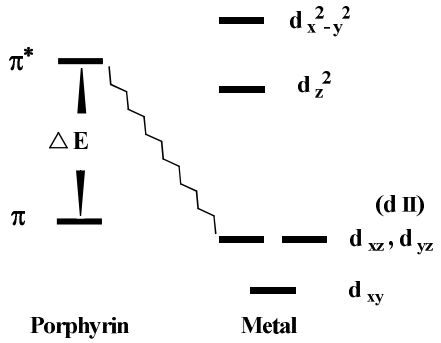

Fig. 8.1: Molecular orbital diagram of Metallo porphyrin

8.2 Experimental [12]

8.2.1 Materials and Methods:

All chemicals and solvents used were of analytical grade reagents. 4-chloro benzaldehyde and pyrrole were from s. d. fine chemicals; propionic acid and methanol (Qualigens) were used without further purification.

8.2.2 Syntheses of compounds:

Scheme: 8.3

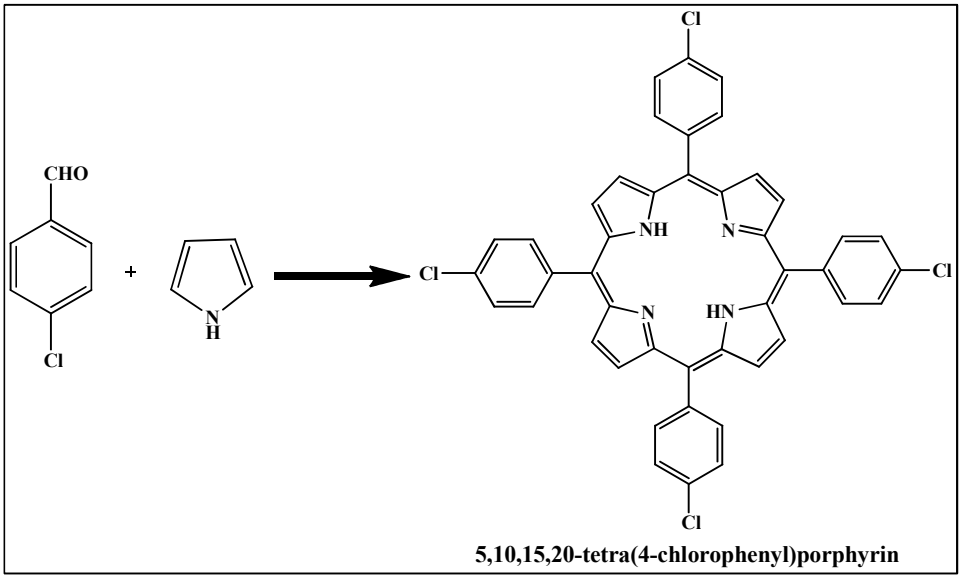

Scheme 8.3: Typical Preparation of 1

8.2.2.1 Preparation of compound 1.

A propionic acid solution (12ml) containing 4-chloro benzaldehyde (0.12ml) and fresh distilled pyrrole (0.08ml) was mixed well and refluxed at 140ºC for 30 mins. After 30 min reaction mixture cooled to room temperature and then 10ml ice cold methanol was added and stirred. Crystallization was induced by scratching the sides of the flask with a glass rod. The deep purple crystals were filtered using a Buchner funnel. The crystals were washed with three 0.5ml portions of cold methanol and three 0.5 ml portions of boiling hot distilled water. The crystals were air dried on high vacuum.

Yield: ~ 12%

Scheme: 8.4

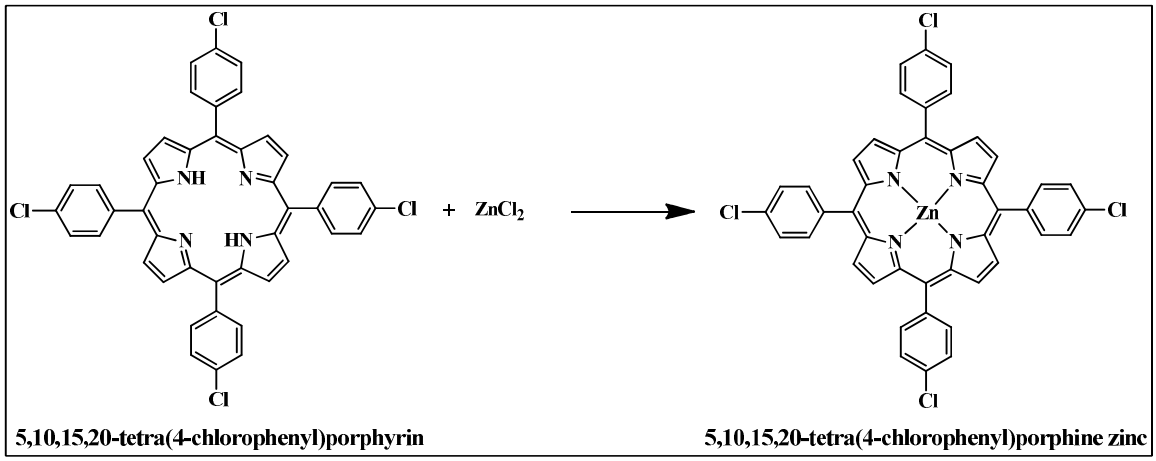

Scheme8. 4: Preparation of Zinc-4-chlorotetraphenyl porphyrin (Zn-1)

8.2.2.2 Preparation of compound Zn-1.

4-ClTPP derivative **1** (2mg) was taken in DMF solution (3mL) and zinc chloride (10mg) was added to the reaction mixture. The reaction mixture was heated to a gentle reflux (at 150°C) for 30 min. After 30 min. reaction mixture was cooled down to room temperature and precipitated solid was filtered. Precipitate washed with DMF and methanol. Purification of metalloporphyrin was carried out using column chromatography (alumina-hexane: ethyl acetate).

Yield: 56.45%

8.3 Result and Discussions

Compounds **1** and **Zn-1** were characterized using elemental analyses, FT-IR, ^{1}H NMR, uv-visible spectrophotometer and fluorescence spectrophotometer.

8.3.1 Elemental analyses:

The calculated elemental analyses were consistent with the observed formulae.

Compound 1: Anal. Calc. for $C_{44}H_{26}Cl_4N_4$: C, 70.23%; H, 3.48%; N, 7.45%; **Found:** C, 70.13; H, 3.18; N, 7.55%.

Compound Zn-1: Anal. Calc. for $C_{44}H_{24}Cl_4N_4Zn$: C, 64.77%; H, 2.96%; N, 6.87%; **Found:** C, 64.69; H, 3.21; N, 6.49%.

8.3.2 FT-IR:

FT-IR spectra of compound **1 and Zn-1** were recorded at RT. Characteristic FT-IR vibrations on compounds **1 and Zn-1** are listed in Table8.1 and shown in Figure 8.2 and Figure 8.3.

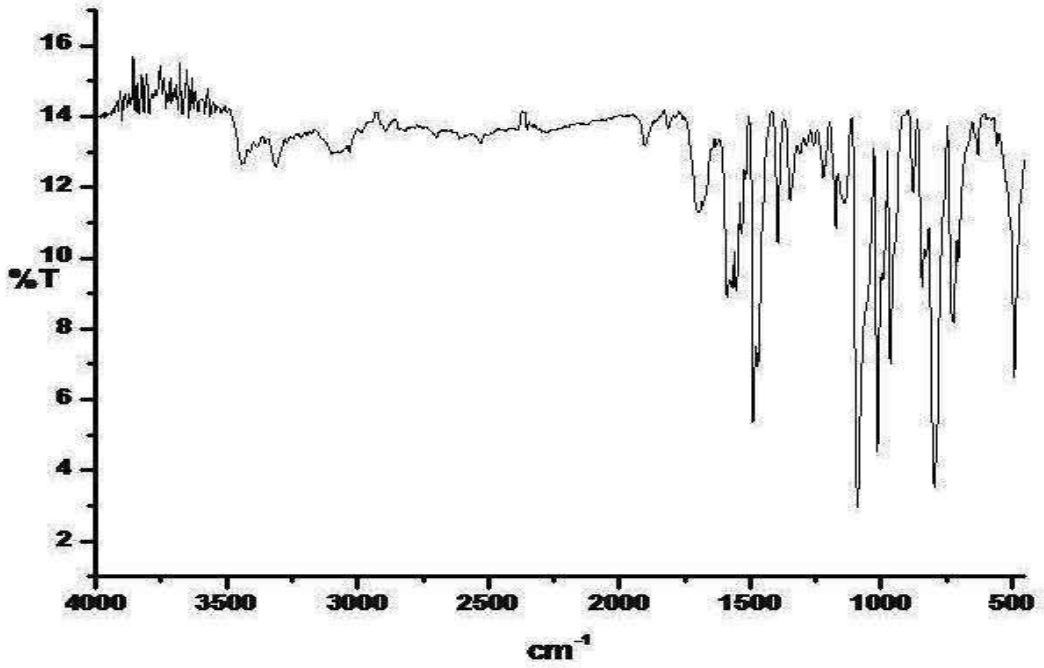

Fig. 8.2: FT-IR Spectrum of compound 1

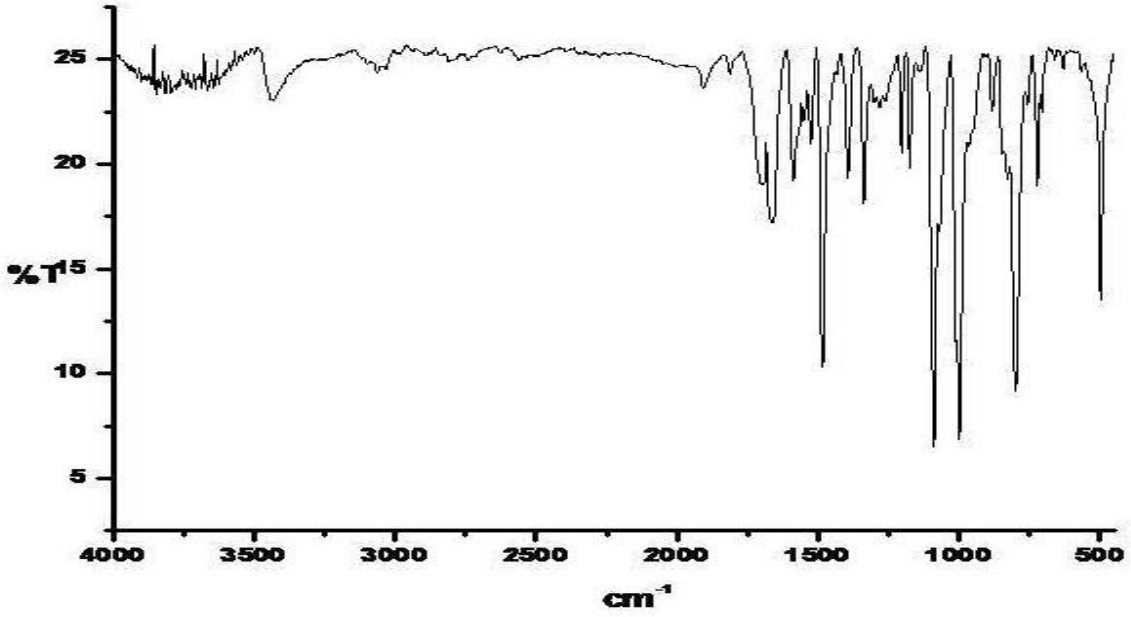

Fig. 8.3: FT-IR Spectrum of compound Zn-1

Table 8.1: FT-IR modes of compounds 1 and Zn-1

Compounds	*ν*N-H (δN-H)	*ν*=C-H	*ν*C=C	*ν*C=N	*γ*=C-H	*ν*Zn-N
1	3315 (965)	3024	1627	1349	796	-
Zn-1	-----	3031	1658	1337	797	993

An IR absorption frequency is different for free base 4-ClTPP (**1**) and Zinc-4-ClTPP complex (**Zn-1**) with different functional groups. It is found that the N-H bond stretching and bending frequencies of free base porphyrin (**1**) located at ~3315 cm^{-1} and ~965 cm^{-1}. When the Zinc ion is inserted into the porphyrin ring, the N-H bond vibration frequency of free base porphyrins disappeared and the characteristic functional group frequency of Zn-N bond is observed around 993 cm^{-1}, which indicates the formation of zinc porphyrin (**Zn-1**) compound. The bands at 2923-3133 cm^{-1} are assigned to the C-H bond of the benzene ring and pyrrole ring as shown in Table.8.1. The bands at 1627-1658 cm^{-1} and 1349-1337 cm^{-1} are assigned to the C=C stretching mode and the C=N stretching vibration respectively. The bands at 800cm^{-1} assigned to the C-H bond bending vibration of *para*-substituted phenyl ring. Generally, the vibration frequency shift to the higher frequency region (blue shift) as the bond energy is increased.

8.3.3 ^{1}H NMR Spectra:

Formation of compound **1** and **Zn-1** has been confirmed by ^{1}H NMR spectroscopy (Figure 8.4a and 8.4b). The details of ^{1}H NMR spectra for all these compounds are tabulated in Table 8.2.

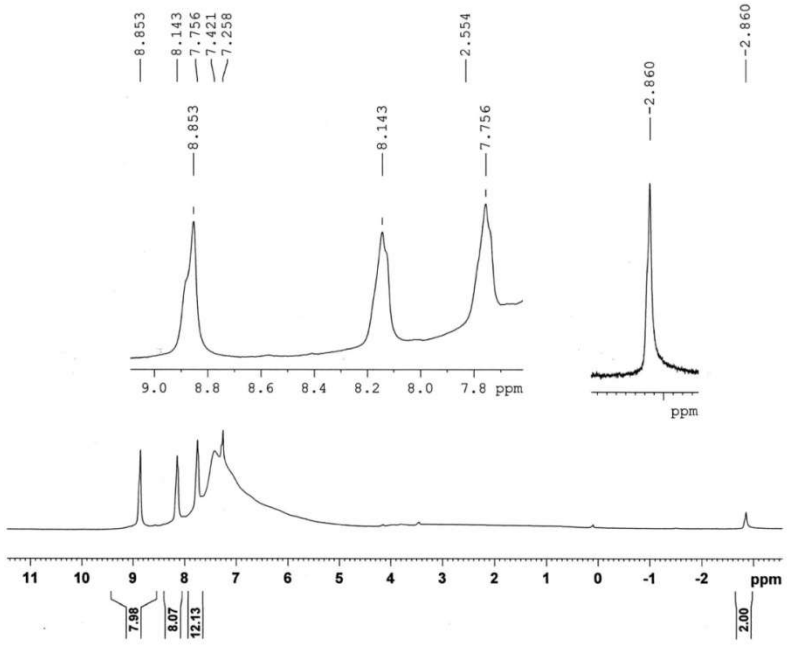

(a)

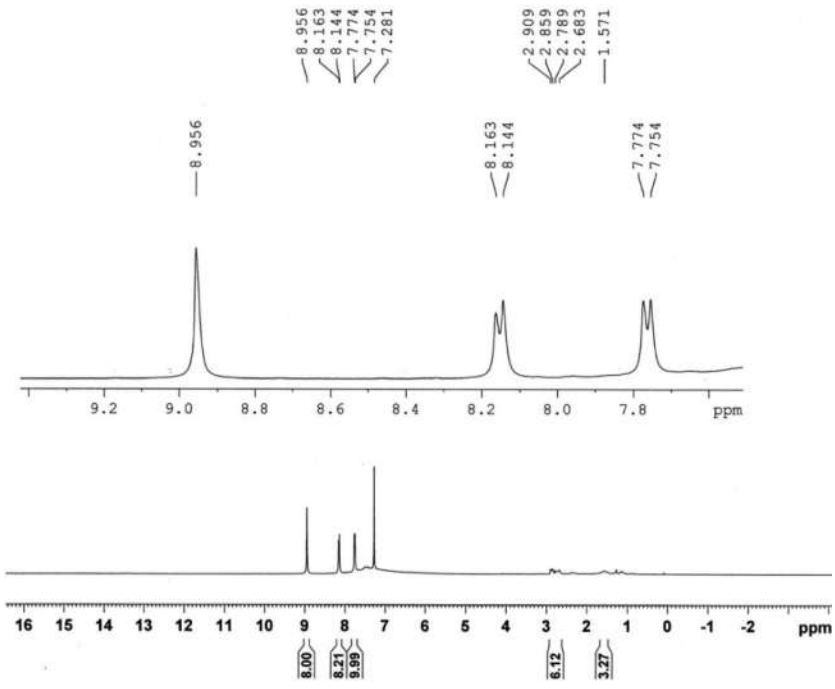

(b)

Fig. 8.4: ^{1}H NMR Spectra of (a) 1 and (b) Zn-1

Table 8.2: ^{1}HNMR data of compounds 1 and Zn-1

Compounds	(δ value) ^{1}H NMR (d6-DMSO) J coupling in Hz
1	8.85 (s, 8H, β-pyrrole-H), 8.14 (d, 8H, $ArH_{2,6}$, J = 8.3 Hz), 7.56 (d, 8H, $ArH_{3,5}$, J = 8.1 Hz), –2.86 (s, 2H, NH).
Zn-1	8.96 (s, 8H, β-pyrrole-H), 8.14-8.16 (d, 8H, $ArH_{2,6}$, J = 8.3 Hz), 7.75-7.77 (d, 8H, $ArH_{3,5}$, J = 8.1 Hz).

It is observed that in the free base porphyrin (**1**), internal N–H protons are highly up field (δ= -2.86 ppm), and β-protons appeared at δ= 8.85 ppm. The *meso*-phenyl protons consist of a *doublet* for the *ortho*-hydrogen's (δ = 8.14 ppm) and another doublet (δ= 7.56 ppm) for the *meta*-protons.

The formation of zinc complex of porphyrin (**Zn-1**) causes disappearance of internal N–H protons and downfield shifts of the β-protons to δ= 8.96 ppm from δ = 8.85 ppm confirms the formation of **Zn-1**. The *meso*-phenyl protons also showed slight downfield shift and consist of a *doublet* for the *ortho*-hydrogen's (δ = 8.14-8.16 ppm) and another doublet (δ = 7.75-7.77ppm) for the *meta*-protons.

8.4 Spectral Information

8.4.1 UV-Visible Spectra:

The UV–Visible spectra consist of two absorptions bands in two different regions. One of the absorption bands appeared in the near-ultraviolet and other one in the visible regions. Porphyrin and metalloporphyrin molecules show an intense B- or Soret band at 390–425 nm and weaker Q-bands show four absorptions for porphyrin and only two for metalloporphyrin in the range of 500–700 nm. The number, intensity and exact location of these bands depend upon the substitution pattern of the macro cycles as well as whether the porphyrin is metallated or not and the kind of metal coordinated by the central cavity. In the present study of compound **1** and **Zn-1**, four and two Q-bands (IV, III, II and I) with different relative intensities and a Soret band have been observed respectively. A typical uv-visible spectrum of **1** and **Zn-1** are shown in Figure 8.5.

Table 8.3: Soret and Q-Bands in compound 1 and Zn-1

Compound	Soret Band(nm)	Q-Bands(nm)			
1	402.00	513.96	548.06	589.59	647.51
Zn-1	429.09, 405.60 (shoulder)		559.04	598.58	

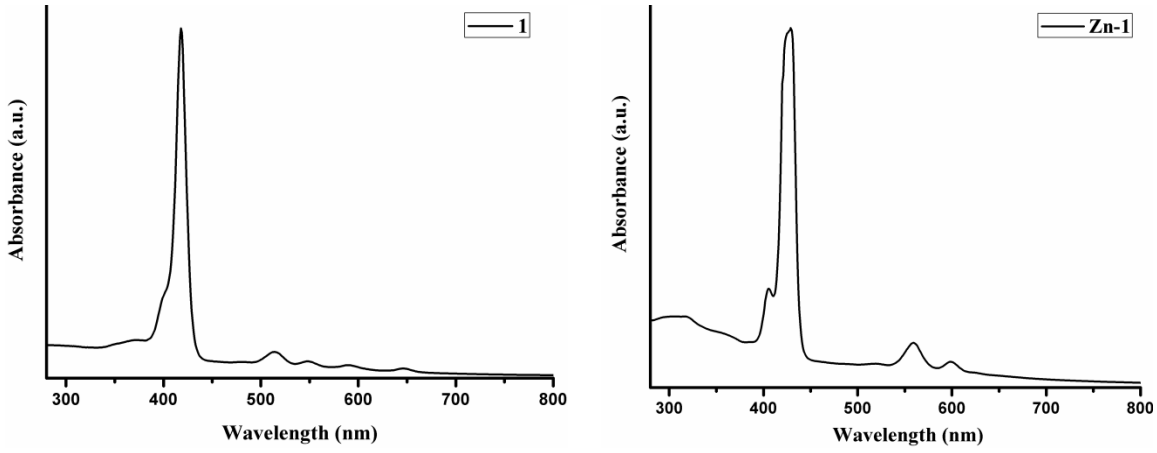

(a) **(b)**

Fig. 8.5: Absorption spectra of (a) 1 and (b) Zn-1

UV-Vis spectra of free base porphyrins (**1**) show Soret band at 402 nm and four Q-bands at 513.96, 548.06, 589.59 and 647.51nm. When the zinc metal ion is introduced into the porphyrin ring, **Zn-1**, then, slight bathochromic shift is observed for Soret band (429.09 nm) and number of the Q bands reduced to two (559.04 and 598.58 nm) with decreased intensity. Appearance of small shoulder band at 405.60 nm, a characteristic of metalloporphyrin is also observed for **Zn-1**. The energy levels of π_1 and π_2 orbits is increased and the energy gap between HOMO and LUMO of the porphyrin ring became smaller. The π-π^* electron excitation of the porphyrin ring require light of smaller energy (longer wavelength), accordingly in the absorption band (Soret band) red shift occur and located in the long wavelength.

8.4.2 Fluorescence spectra

A typical emission spectrum for compound **1** and **Zn-1** are shown in Figure 8.6 and listed in Table 8.4.

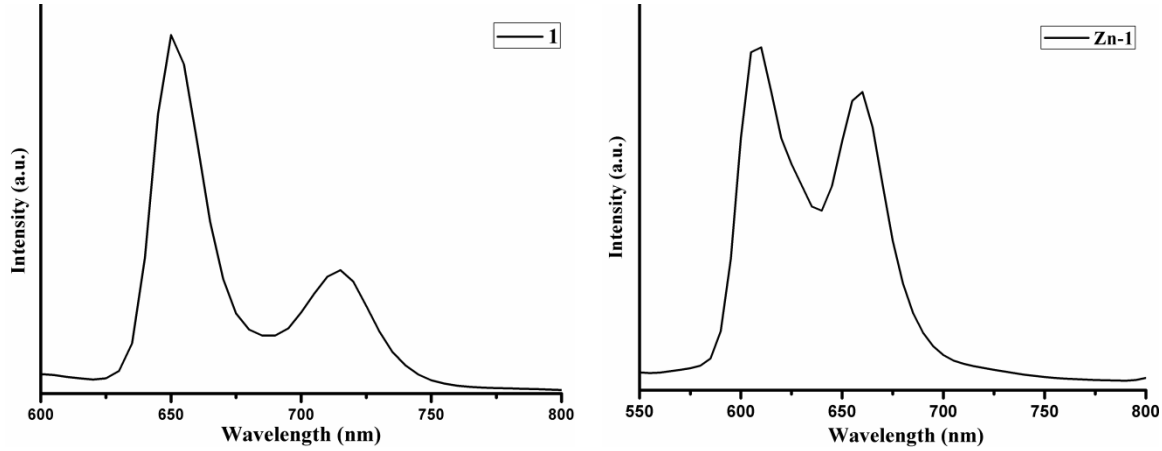

Fig. 8.6: Fluorescence study of (a) 1 and (b) Zn-1

Table 8.4: Emission bands of 1 and Zn-1.

Sr. No.	Compounds	F1 λ_f^{max} (nm)	F2
1	**1**	649	720
2	**Zn-1**	608	660

Two fluorescence bands are observed in case of **1** and **Zn-1** after excitation with 402 nm and 429nm respectively which are usually assigned as F1 and F2. **1** gives fluorescence emission maxima (F1 and F2, λ_f^{max}) at 649 nm and at 720 nm. Upon metallation (**Zn-1**), the porphyrin ring system deprotonates, forming a dianionic ligand, hypsochromic emission shift is observed at 608 nm and 660 nm. The metal ions behave as Lewis acids, accepting lone pairs of electrons from the dianionic porphyrin ligand. Unlike most transition metal complexes, their color is due to absorption(s) within the porphyrin ligand involving the excitation of electrons from π to π* porphyrin ring orbital's. The change in the spectrum (fewer peaks) on metallation is due to increased symmetry relative to the free-base porphyrin .The two hydrogen on the nitrogen atoms in the free base porphyrin reduce the ring symmetry from square (for metalloporphyrin) to rectangular- that is, from D_{4h} to $D_{2h.}$

Part-II: Studies on Nanoparticles: TPP, Metallo-TPP and CdS

8.5 Introduction

The cadmium sulfide (CdS) is an important II–VI semiconductor (E_g = 2.42 eV; 515 nm at room temperature) has many applications in multiple technical fields including photochemical catalysis, gas sensor, detectors for laser and infrared, solar cells, nonlinear optical materials, various luminescence devices, optoelectronic devices and so on [13]. It is also most promising candidate among II-VI compounds for detecting visible radiation. In last decade, efforts have been devoted to the preparation of high - quality CdS nanoparticles for investigating optical properties. The possibility of tuning these properties by controlling the size and shape implies search of new experimental methodologies and characterization techniques. To name a few, sea-urchin like cadmium sulfide nanoparticles with nanorod-based architecture were prepared by solvothermal method, with cadmium chloride and thiourea in ethylenediamine solution, the CdS nanoparticles have been assembled into CdS nanorods and arrayed nanorods bundles by a thioglicolic, cadmium sulfide nanorods were also synthesized in micro-emulsions formed by non-ionic surfactants.

Although, investigation on CdS nanoparticle with various porphyrin/ metalloporphyrins is well reported [14], its interaction with nanosized porphyrin/metalloporphyrins is not under taken? What will happen if organic counterpart (porphyrin/ metalloporphyrins) also present in nanoparticle size? Will interaction at nano-nano level differ?

On this background, we observed Kulkarni et.al. reported the interaction between CdSe nanoparticles and ZnTPP nanoparticles, where fluorescence enhancement of latter at the cost of the fluorescence due to former nanoparticles is observed. Here we observed completely opposite outcome.

We report the fluorescence quenching of **1NP**/ **Zn-1NP** in presence of colloidal CdS due to formation of nanocomposite. The nanocomposite formed has particle size around 5-12 nm, and need detailed investigation. The fluorescence measurement has been used as a tool to study the interaction between nano porphyrins and CdS nanoparticles.

8.6 Experimental

8.6.1 Materials and Methods:

All chemicals were of analytical grade reagents. Polyacrylamide (PAM), CTAB and starch were from Sigma-Aldrich; Triethylene glycol monomethyl ether and PEG (10000) from s.d. fine chemicals; doubly deionized water was used for the preparation. Hydrogen sulphide gas was generated in Kipp's apparatus by mixing iron (II) sulphide and hydrochloric acid.

8.6.2 Preparation of nanoparticles and nanocomposite:

The nanoparticles syntheses were tried using various stabilizers in which polyacryalmide gave better result as shown in Table 8.5.

Scheme: 8.5

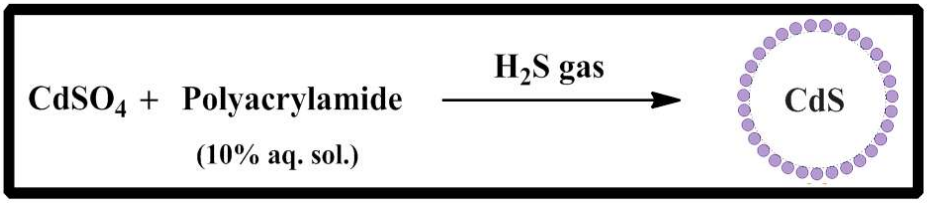

Scheme 8.5: Preparation of CdS nanoparticles (3NP)

8.6.2.1 Preparation of CdS nanoparticles (3NP) [15]:

CdS nanoparticles were prepared by using $CdSO_4$ (1×10^{-4} M, 0.4 mL) and 10% aq. Polyacrylamide (4 mL) solution. Hydrogen sulphide gas was passed through this solution for few seconds (10-15s) with continuous stirring at room temperature. The reaction mixture was stirred for few minutes to obtain yellow fluorescent solution. The solution analyzed with DLS, UV and fluorescence spectroscopy for investigation.

Scheme: 8.6

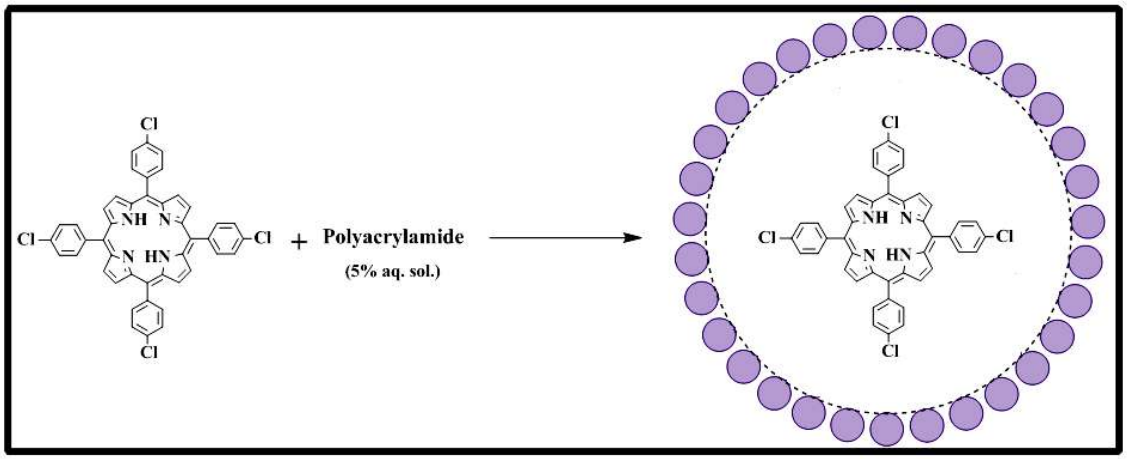

(a)

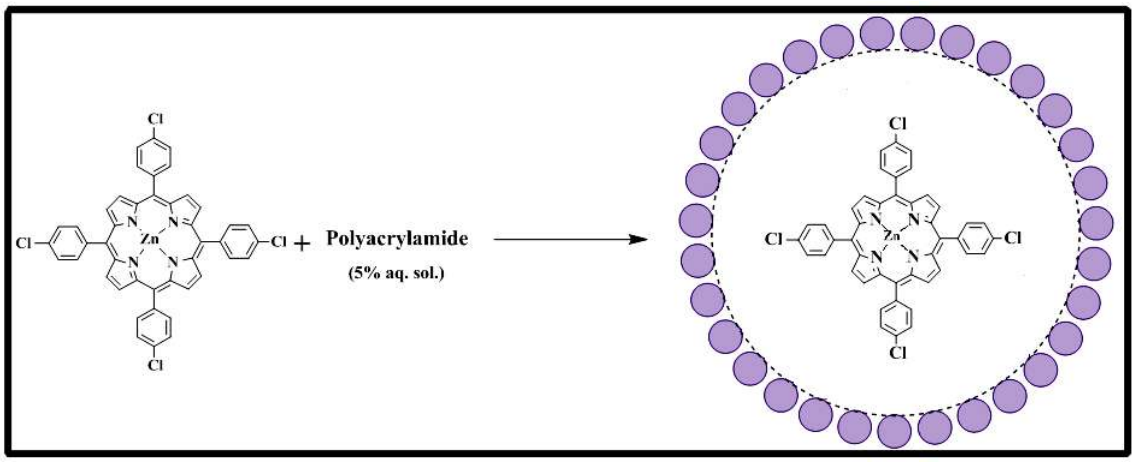

(b)

Scheme 8.6: (a) Preparation of T (p-Cl) PP nanoparticles (1NP); (b) Preparation of Zn- T (p-Cl) PP nanoparticles (Zn-1NP).

8.6.2.2 Preparation of T (p-Cl) PP and Zn- T (p-Cl) PP nanoparticles (1NP and Zn-1 NP) [16]:

1NP/ **Zn-1NP** particles were prepared by means of following procedure: stabilizer (5% aq. Polyacrylamide, 0.05mL) was added to stock solution of **1**/ **Zn-1** in DMF (0.4 mL), followed by addition of water (5 mL) with vigorous stirring. The solutions were analyzed for DLS, UV and fluorescence spectroscopy to identify the presence of nanoparticles.

8.6.2.3 *in-situ* Preparation of T (*p*-Cl) PP nanocomposite (1NC) and Zn- T (*p*-Cl) PP nanocomposite (Zn-1NC) with CdS nanoparticles.

Stock solution of **1/ Zn-1** (0.4mL) in DMF and $CdSO_4$ (0.4 mL) aq. solution were transferred to the beaker followed by the addition of 10% aq. Polyacrylamide (0.05 mL) and 5% aq. Polyacrylamide (0.05mL) solution. After 1 minute, 5ml water was added to this mixture with vigorous stirring. Hydrogen sulphide gas was passed through this solution for few seconds (10-15s) with continuous stirring at room temperature. The solutions were analyzed for DLS, UV and fluorescence spectroscopy to identify the presence of nanoparticles.

8.7 Result and Discussions

1NP/ **Zn-1NP** particles were tried using different stabilizers (Table 8.5) out of polyacryalmide gave the better size of nanoparticles. Hence polyacryalmide stabilizer was selected for further study.

Mixing of nanoparticle solutions of **3NP** and **1NP**/ **Zn-1NP** i.e. *ex-situ* preparation resulted in more than 100 nm size of composite, hence *in-situ* preparation was preferred for further studies.

8.7.1 Dynamic Light Scattering (DLS):

Nanoparticle preparation of 1, Zn-1, CdS and nano-composites in presence of various stabilizers lead to different sizes during DLS studies are tabulated in Table8.5. Figure 8.7 shows lowest size of CdS nanoparticles (15 nm), 1NP (101 nm) and **Zn-1NP** (86 nm) in polyacrylamide. Figure 8.8 shows size distributions of nano-composites synthesized using *ex-situ* and *in-situ* methods.

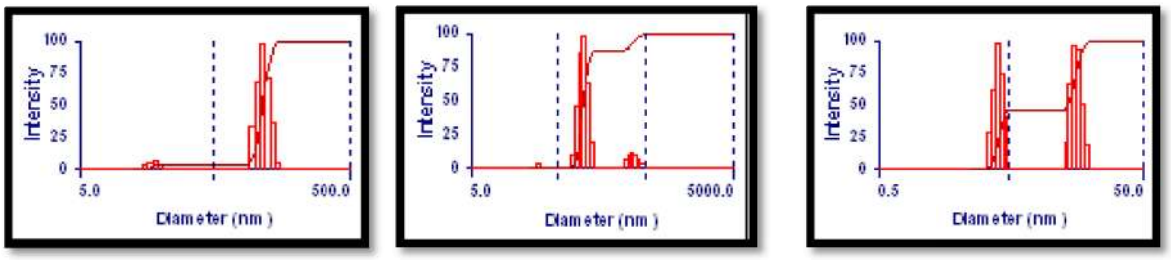

(a) **(b)** **(c)**

Fig. 8.7: charts indicating particle size of 1NC, Zn-1NC and 3NC in solution using polyacryalmide stabilizer.

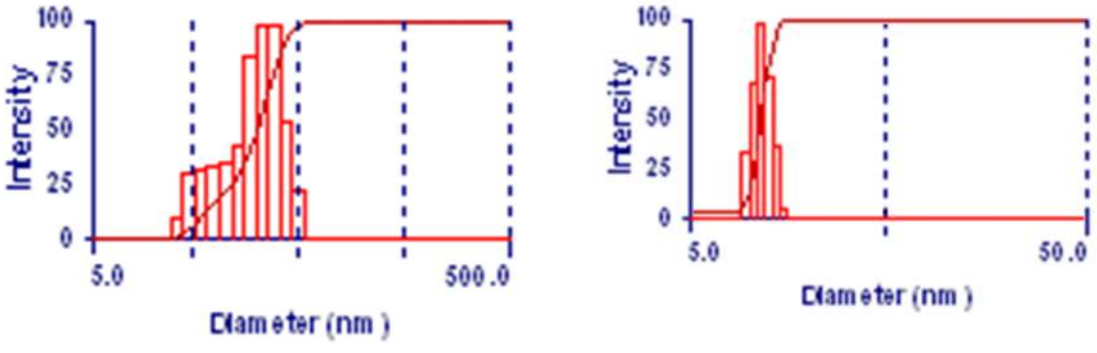

ex-situ *in-situ*

Fig. 8.8: charts indicating particle size of 1NC (*ex-situ*) and 1NC (*in-situ*) in solution using polyacryalmide stabilizer.

Table 8.5: Study with different Stabilizers and particle size of compound 1NP, Zn-1NP, 3NP, 1NC and Zn-1NC.

Stabilizer	Size of 1NP	Size of Zn-1NP	Size of CdS (3NP)	Size of Nanocomposite (1NC)	Size of Nanocomposite (Zn-1NC)
Starch	700 nm	780 nm	500 nm	>1000 nm	>1000 nm
CTAB	250 nm	300 nm	340 nm	>1000 nm	>1000 nm
Triethylene glycol monomethyl ether	120 nm	108 nm	160 nm	500 nm	500 nm
PEG (10000)	340nm	600 nm	705 nm	>1000 nm	>950 nm
Polyacrylamide (*ex-situ*)	101nm	86 nm	15 nm	150-200 nm	100-130 nm
Polyacrylamide *(in-situ)*		NA		9-12 nm	

8.7.2 UV-Visible Spectra

8.7.2.1 UV-Visible spectra of CdS and CdS nanoparticles (3)

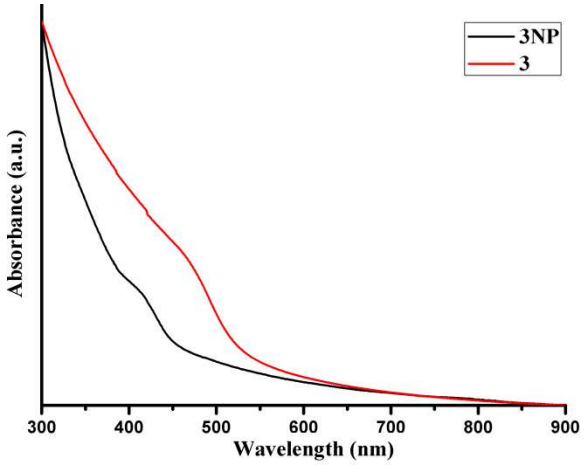

Fig. 8.9: Absorption spectra of CdS and its nanoparticles in polyacryalmide

UV-Vis absorption spectra of bulk cadmium sulfide (Figure 8.9) showed maxima at 515 nm [17]. Nanosized CdS particles **3** obtained with polyacryalmide as stabilizer (i.e. quantum dots) showed intense absorption maxima at 457 nm which is relatively blue shifted with respect to the band gap of bulk CdS particles. These are first excitonic states of CdS nanoparticles; the nanoparticle band gap energy is higher in energy relative to bulk material. This blue shifted wavelength from absorbance studies is used to calculate band gap of CdS nanoparticles using following equation 1.

$$\Delta E = E_{NP} - E_{BULK} = hc/\lambda - E_{BULK} \quad \text{..... (1)}$$

Where, E_{NP} = band gap energy of CdS nanoparticles; E_{NP} = band gap energy of bulk CdS (2.42eV); λ = wavelength of absorbance; h= Planck's constant (6.62606957 × 10^{-34} m^2 kg / s); c= speed of light (3.00 x 10^8 m/s). Band gap energy of CdS nanoparticles from fig.8.9 is 2.71 eV which give ΔE value of 0.29 eV. This ΔE difference can be correlated to particle size using Brus equation as shown in equation 2.

$$\Delta E = \pi^2 h^2 / 2R^2 \, (1/m_e + 1/m_h) - (3.6e^2/4\pi\varepsilon d_p) \quad \text{..... (2)}$$

By solving this equation, calculated particle size of CdS nanoparticles (**3**) is 3.65 nm which approximately matches with the particle size from DLS result.

8.7.2.2 UV-Visible spectra of 1NP, 1NC, Zn-1NP and Zn-1NC

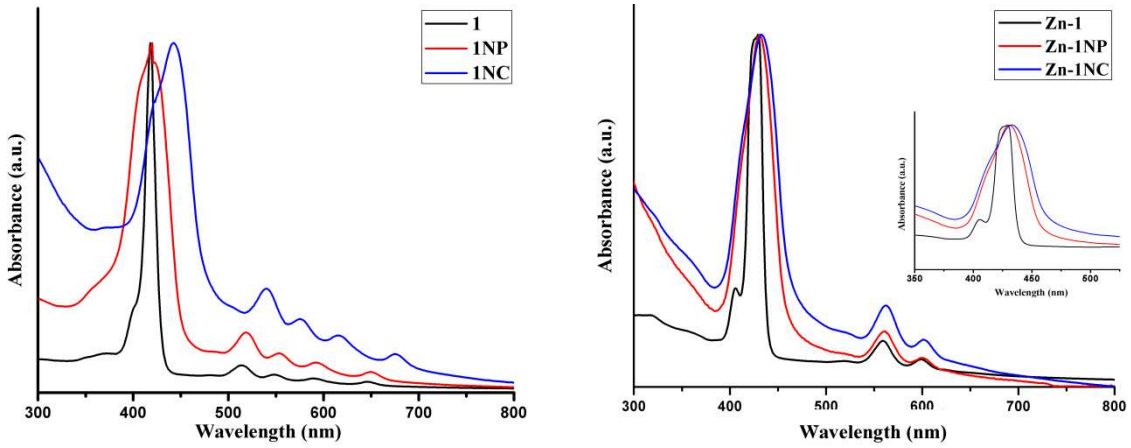

(a) **(b)**

Fig. 8.10: Normalized absorption Spectra of (a) 1/ 1-NP / 1-NC. (b) Zn-1 / Zn-1NP / Zn-1NC.

Table 8.6: Shift in Soret and Q-Bands of Nanocomposite

	UV-Vis. (nm)					
Sample Name	**Soret Band**		**Q-Bands**			
1	402	418.16	513.96	548.06	589.59	647.51
1-NP	356	419	518	553	592	649
1-NC	--	445	542	577	619	671
Zn-1	405.60	429.09	--	559.04	598.58	--
Zn-1-NP	410.41	435.62	--	561.95	602.26	--
Zn-1-NC	410.15	433.52	--	562.07	601.63	--

The UV-visible spectra of porphyrin nanoparticles are significantly different compared to the spectra of the corresponding porphyrin solutions. Figure 8.10- (a) and (b) show the absorption spectra of **1NP** and **Zn-1NP**. Soret bands in **1NP** and **Zn-1NP** are found to be broadened and/or split confirms the formation of nanoparticles. During formation of **1NP** from **1**, Soret band get broadened and peak at 402 nm showed hypsochromic shift to 356 nm. On the other hand, Soret band becomes broader during conversion of **Zn-1** to **Zn-1NP**. Q-bands of both **1NP** and **Zn-1NP** show slight bathochromic shift compared to that of **1** and **Zn-1**. The values of shift are tabulated in Table-8.6**.**

Interestingly, addition of CdS (*in-situ*) to obtain nanocomposite, **1NC** and **Zn-1NC**, results in bathochromic shift in Soret band in **1NC** while small hypsochromic shift in **Zn-1NC**. The absorption maxima 419 nm for **1NP** get red shifted to 445 nm for **1NC**, on the other hand absorption maxima at 436 nm for **Zn-1NP** gets blue shifted to 433 nm in **Zn-1NC** composite.

Q bands in **1NC** also showed major bathochromic shift for all four bands while small bathochromic shift is observed in **Zn-1NC**. The *Q* bands of **1NP** were red shifted to 542 nm, 577 nm, 619 nm and 671 nm from 518 nm, 553 nm, 592 nm and 649 nm while **Zn-1NP** *Q* bands do not shift. These changes in absorption spectra clearly indicate that the formation of **1NC**/ **Zn-1NC** composites with presence of **1NP**/ **Zn-1NP** as well as colloidal CdS nanoparticles.

8.7.3 Fluorescence spectra

8.7.3.1 Fluorescence spectra of CdS nanoparticles (3)

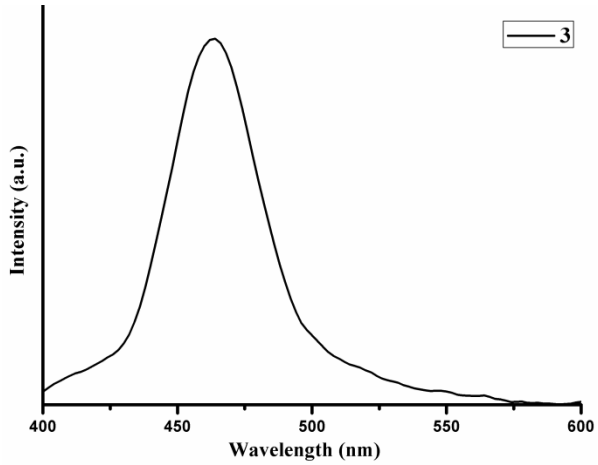

Fig. 8.11: Fluorescence spectra of 3

The fluorescence of CdS particles (**3**) get quenched when nanoparticles formation took place. As the surface of NP is covered by the stabilizer the fluorescence intensity get quenched. The observed broad and weak emission peak at 464 nm is assigned to the trapped luminescence i.e. recombination of charged carriers trapped in the surface states related to the size of CdS nanoparticles [18]. Figure 8.11 also depicts that the absorption spectra of **1NP** (Figure 8.10a) and **Zn1-NP** (Figure 8.10b) overlaps with the fluorescence spectrum of **3,** an essential condition for the energy transfer from **3NP** (CdS NP) to **1NP** and **Zn1-NP** by the fluorescence resonance energy transfer process [19].

8.7.3.2 Fluorescence spectra of 1NP, 1NC, Zn-1NP and Zn-1NC

Figure 8.12- a/b shows a fluorescence spectrum (excitation by 405 nm) of **1NP**/**Zn-1NP** nanoparticles along with that of **1**/Zn-**1** solution (0.25 mM).

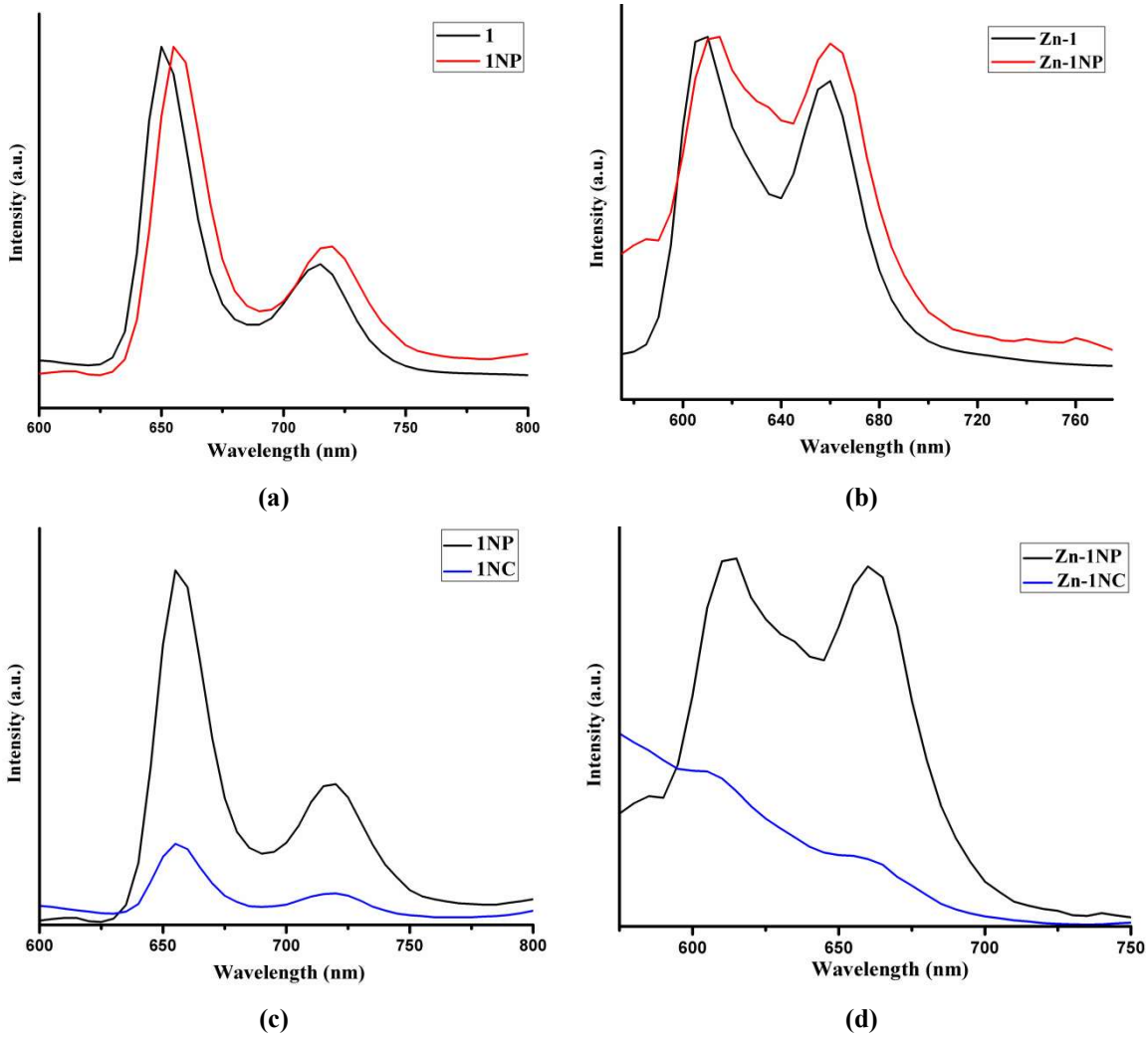

Fig. 8.12: Comparison between fluorescence spectra of (a) 1 and 1NP, (b) Zn-2 and Zn-1NP, (c) 1NP and 1NC and (d) Zn-2NP and Zn-1NC .

Two fluorescence bands (F1 and F2) also observed in **1NP** and **Zn1-NP** which are slightly red-shifted (bathochromic shift), F1 by 4 nm and F2 by 3 nm corresponding to the behavior observed in the absorption spectra (limit of detection for our instrument). Addition of stabilizer slightly quenches the fluorescence of solution-phase **1NP** and **Zn-1NP** further. Reason behind this may be particles are covered with stabilizer and increase in dilution factor of solution.

The effects of the presence of colloidal CdS (**3**) on the fluorescence spectra **1NP/ Zn-1NP** nanoparticles in nanocomposite were also examined. Fig.8.12c/d shows the fluorescence spectra **1NC**/**Zn-1NC** nanocomposite excitation at 405nm. As seen, addition of CdS results into total fluorescence quenching of **1**/**1NP** and **Zn-1**/**Zn-1NP**. The fluorescence bands (F1 and F2) of **Zn-1**/**Zn-1NP** are slightly blue shifted by 2–4 nm in **Zn-1NC** composite. In both samples of **1NC** and **Zn-1NC,** no precipitation was observed even after several hours of mixing CdS (**3NP**) with **1NP** and **Zn-1NP** respectively. These results point toward that formation of nanocomposite (**1NC** and **Zn-1NC**) is stable and has no fluorescence.

8.7.4 Cyclic Voltametry

In the present study, the oxidation potential of **1**, **1NP**, **1NC**, **Zn-1**, **Zn-1-NP** and **Zn-1-NC** were measured in DMF-water with sodium chloride (0.1 M) as electrolyte. The experimental setup consisted of a platinum working electrode, a glassy carbon counter electrode and a silver reference electrode. Reversible peak potentials were measured at different scan rates (0.03 V/s). All samples were deaerated by bubbling with pure nitrogen gas for ca. 5 min at room temperature.

Table 8.7: Photo physical properties of all compounds such as excited state energy (Es), ground (Es/s+) and excited state oxidation potential (Es∗/s+)

Sr. No.	Compounds	λ_f^{max} (nm)	E_s (eV)[a]	$E_{s/s+}$ (eV)[b]	$E_{s*/s+}$ (eV)[c]
1	**1**	649, 849	1.91	1.49	-0.42
2	**1-NP**	655, 718	1.89	1.47	-0.42
3	**1-NC**	655, 718	1.89	1.44	-0.45
4	**Zn-1**	608, 660	2.04	1.49	-0.55
5	**Zn-1-NP**	613, 660	2.02	1.43	-0.59
6	**Zn-1-NC**	606, 658	2.04	1.42	-0.62

[a] E_S -Singlet state energy of the porphyrins calculated from the fluorescence maximum wavelength [20].

[b] $E_{s/s+}$ - The oxidation potentials of the ground state porphyrin are in DMF-water vs NHE from cyclic voltametry measurements.

[c] $E_{s*/s+}=E_{s/s+}-E_s$, where $E_{s*/s+}$ is the oxidation potential of the singlet excited state porphyrins

Fluorescence emission quenching may happened due to (i) energy transfer, (ii) electron transfer and/or (iii) formation of complex which has no fluorescence emission (exciplex). Band-gap energy of CdS semiconductor (Eg= 2.71 eV) is much greater than the excited state energy of **1**/**Zn-1** (Es) (Table 8.7). Hence, fluorescence emission of the **1**/**Zn-1** cannot be absorbed by the colloidal CdS (**3NP**) ruling out the possibility of energy transfer from the excited state of **1**/**Zn-1** to colloidal CdS.

The second possible mechanism of fluorescence emission quenching of **1**/**Zn-1** in **1NC**/**Zn-1NC** by colloidal CdS (**3**) is due to electron transfer. It occurred due to difference between excited state oxidation potential of **1**/**Zn-1** and energy level of the conduction band potential of CdS (**3**) as shown in the following equation.

$$\textbf{TClPP/Zn-TClPP* (S1) + CdS} \longrightarrow \textbf{TClPP/Zn-TClPP}^{+} + \textbf{CdS(e)}_{\textbf{sens}}$$

Oxidation potential of excited singlet (Table 8.7) of **1**/**Zn-1** can be obtained using equation $E_{s*/s+}=E_{s/s+}-E_s$. These energy levels are energetically much higher than the energy level of the conduction band of CdS (−1.0 V vs NHE)[28]. Hence thermodynamically electron-transfer path is impossible as shown in Scheme 8.7.

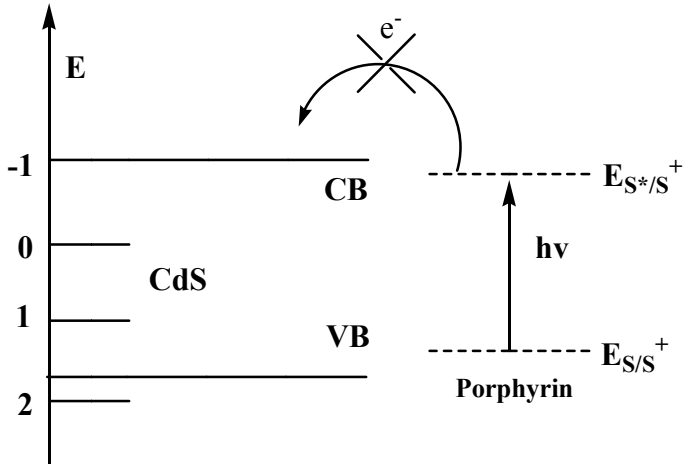

Scheme 8.7: Electron transfer from the excited state of Porphyrins to the conduction band of CdS

In conclusion, fluorescence quenching can be attributed to formation of complex-composite (Figure 8.13) in the excited state between CdS colloid (**3NP**) and **1NC**/**Zn-1NC** with no fluorescence.

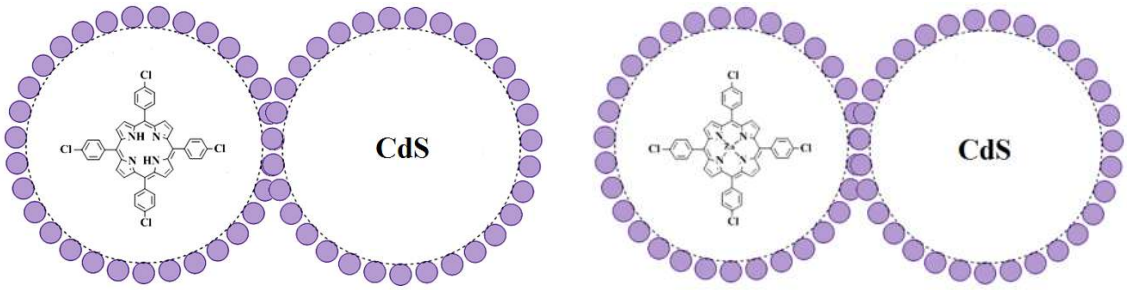

Fig. 8.13: CdS colloids surface interaction with (a) 1NC, (b) Zn-1NC

This can be represented by equations as shown in scheme 8.7a/b.

$$\mathbf{1NP + CdS} \rightleftharpoons \mathbf{[1NP\text{---}CdS] \equiv 1NC} \qquad \text{------ (a)}$$

$$\mathbf{Zn\text{-}1NP + CdS} \rightleftharpoons \mathbf{[Zn\text{-}1NP\text{---}CdS] \equiv Zn\text{-}1NC} \qquad \text{------ (b)}$$

Scheme 8.7: Formation of exciplex (a) 1NC; (b) Zn-1NC

8.8 Conclusion

- Synthesized and characterized *5,10,15,20*-tetra (4-chlorophenyl*)*porphyrin (**1**) and *5,10,15,20*-tetrakis(4-chlorophenyl*)*porphyrin-Zn(II) - (**Zn-1**) using elemental analyses, FT-IR, ^{1}H NMR, UV-Visible spectroscopy and fluorescence spectroscopy.

- Nanoparticles of **1**, **Zn-1** and CdS (**3**) have been synthesized and characterized using UV-Visible, Emission Spectroscopy and DLS.

- *In situ* nanocomposite formation was carried out using polyacryalmide as stabilizer been successfully synthesized and characterized by using DLS, UV and fluorescence spectroscopy.

- Total fluorescence quenching of **1NC/Zn-1NC** is due to excited state (exciplex) complex ((**1NP**/**Zn-1NP**) --- **CdS)** formation.

8.9 References

[1] B. O'regan, M. Grfitzeli, *Nature* **1991**, *353*, 737-740; (b) J. Zhang, R. O'Neil, T. Roberti, *J.Phys.Chem.***1994**, *98*, 3859-3864.

[2] C. Chen, X. Qi, B. Zhou, *J. Photochem. Photobiol. A: Chem.* **1997**, *109*, 155-158.

[3] (a) Y. Zhang, H. Dong, Q. Tang, S. Ferdous, F. Liu, S. C. B. Mannsfeld, W. Hu, A. L. Briseno, *J. Am. Chem. Soc.* **2010**, *132*, 11580-11584; (b) X. Wang, J. Yan, Y. Zhou, J. Pei, *J. Am. Chem. Soc.* **2010**, *132*, 15872-15874.

[4] A. Hagfeldt, M. Graetzel, Acc. Chem. Res. 33 (2000) 269; (b) D. Norris, M. Bawendi, L. Brus, in: J. Jortner, M. Ratner (Eds.), Molecular Electronics, Blackwell Science, Oxford, **2002**, 281.

[5] A. Sukhanova, J. Devy, L. Venteo, H. Kaplan, M. Artemyev, V. Oleinikov, D. Klinov, M. Pluot, J. H. M. Cohen, I. Nabiev, *Anal. Biochem.* **2004**, *324*, 60-67.

[6] (a) K. Kalyanasundaram, N. Vlachopoulos, V. Krishnan, A. Monnier, M. Grätzel, *J. Phys. Chem.* **1987**, *91*, 2342-2347; (b) C. Mou, D. Chen, X. Wang, B. Zhang, T. H. Houwen Xin, F.-c. Liu, *Chem. Phys. Lett.* **1991**, *179*, 237-242.

[7] (a) D. Mauzerall, *Biochemistry* **1965**, *4*, 1801-1810; (b) X. He, Y. Zhou, Y. Zhou, M. Zhang, T. Shen, *J. Colloid Interface Sci.* **2000**, *225*, 128-133.

[8] M. Rahman, H. J. Harmon, *Spectrochim. Acta, Part A: Molecular and Biomolecular Spectroscopy* **2006**, *65*, 901-906.

[9] Z. R. Grabowski, K. Rotkiewicz, W. Rettig, *Chem. Rev.* **2003**, *103*, 3899-4032.

[10] Y. Watanabe, In The Porphyrin Handbook; Kadish, KM; Smith, KM; Guilard, R., Eds, Academic Press: San Diego, **2000**.

[11] E. Austin, M. Gouterman, *Bioinorganic Chemistry* **1978**, *9*, 281-298.

[12] D. Marsh, L. Mink, *J. Chem. Educ.* **1996**, *73*, 1188.

[13] (a) S. Shiojiri, T. Hirai, I. Komasawa, *Chem. Commun.* **1998**, 1439-1440; (b) K. Murakoshi, H. Hosokawa, M. Saitoh, Y. Wada, T. Sakata, H. Mori, M. Satoh, S. Yanagida, *J. Chem. Soc., Faraday Trans.* **1998**, *94*, 579-586; (c) J. Britt, C. Ferekides, *Appl. Phys. Lett.* **1993**, *62*, 2851-2852; (d) S. Schmitt-Rink, D. S. Chemla, D. A. B. Miller, *Advances in Physics* **1989**, *38*, 89-188; (d)W. Qingqing, X. Gang, H. Gaorong, *J. Solid State Chem.* **2005**, *178*, 2680-2685.

[14] M. A. Jhonsi , A. Kathiravan , R. Renganathan *Spectrochim. Acta Part A* **2008**, *71*, 1507–1511.

[15] P. K. Khanna, R. Gokhale, V. V. V. S. Subbarao, *Mater. Lett.* **2003**, *57*, 2489-2493.

[16] X. Gong, T. Milic, C. Xu, J. D. Batteas, C. M. Drain, *J. Am. Chem. Soc.* **2002**, *124*, 14290-14291.

[17] W. Xu, Y. Wang, R. Xu, S. Liang, G. Zhang, D. Yin, *J Mater Sci* **2007**, *42*, 6942-6945.

[18] G. D. Brabson, Z. Mielke, L. Andrews, *J. Phys. Chem.***1991**, *95*, 79-86.

[19] (a) A. R. Clapp, I. L. Medintz, J. M. Mauro, B. R. Fisher, M. G. Bawendi, H. Mattoussi, *J. Am. Chem. Soc.* **2003**, *126*, 301-310; (b) N. Lihitkar, S. Singh, J. Singh, O. Srivastava, R. Naik, S. Kulkarni, *Chem. Phys. Lett.* **2009**, *483*, 227-232.

[20] E. J. Shin, D. Kim, *J. Photochem. Photobiol. A: Chem.***2002**, *152*, 25-31.